EUROPEAN ORGANIZATION FOR NUCLEAR RESEARCH

CERN-EP/80-25 Rev.
18 April 1980

CHARGED BARYON AND ANTIBARYON PRODUCTION IN THE FRAGMENTATION REGION BY 240 GeV PROTONS

[Bristol[1])-Geneva[2])-Heidelberg[3])-Orsay[4])-Rutherford[5])-Strasbourg[6]) Collaboration]

M. Bourquin[2]), R.M. Brown[5]), Y. Chatelus[6]), J.C. Chollet[4]), A. Degré[6]), D. Froidevaux[4]), A.R. Fyfe[1]), J.-M. Gaillard[4]), C.N.P. Gee[5]), W.M. Gibson[1]), P. Igo-Kemenes[3]), P.W. Jeffreys[1],*), B. Merkel[4]), R. Morand[6]), H. Plothow**), J.-P. Repellin[4]), B.J. Saunders[5]), G. Sauvage[4]), B. Schiby[6]), H.W. Siebert[3]), V.J. Smith[1]), K.-P. Streit[3],*), R. Strub[6]), J.J. Thresher[5]) and S.N. Tovey***)

ABSTRACT

Measurements of the production in p-BeO collisions of charged baryons and antibaryons with strangeness between -3 and +3 at $\sqrt{s}$ = 21.2 GeV, x = 0.48, and p_T = 600 MeV/c are reported. The experimental results can be interpreted within the framework of a simple proton fragmentation-recombination model.

(Submitted to Zeitschrift für Physik)

---

1) H.H. Wills Physics Laboratory, University of Bristol, England.
2) University of Geneva, Switzerland.
3) Physikalisches Institut, Universität Heidelberg, Fed. Rep. Germany†.
4) Laboratoire de l'Accélérateur Linéaire, Orsay, France.
5) Rutherford Laboratory, Chilton, Didcot, England.
6) Division des Hautes Energies, CRN, Strasbourg, France.
*) Now at CERN, Geneva, Switzerland.
**) CERN, Geneva, Switzerland; now at LAL, Orsay, France.
***) University of Melbourne, Australia, and CERN, Geneva, Switzerland.
†) Work supported by the Bundesministerium für Forschung und Technologie, Fed. Rep. Germany.

1. INTRODUCTION

Measurements of inclusive charged particle production cross-sections in the CERN Super Proton Synchrotron (SPS) charged hyperon beam have already been published [1]. We report here a new set of measurements (made with the same apparatus) of the production of the antibaryons $\bar{p}$, $\bar{\Sigma}^{\pm}$, $\bar{\Xi}^{-}$, $\bar{\Omega}^{-}$ and of the corresponding baryons. The hyperon beam [1] was tuned to select particles with an average momentum of 113 GeV/c, produced at an angle of 5.3 mrad by 240 GeV protons interacting in a 32 cm long BeO target. The non-zero production angle of 5.3 mrad, corresponding to an average transverse momentum p_T = 600 MeV/c, was needed for the positive polarity runs in order to obtain sufficient separation between the proton beam and the secondary beam at the first collimator. The same value of the production angle was used for negative polarity runs in order to make a direct comparison of particle and antiparticle production under the same kinematic conditions.

2. PARTICLE FLUXES AND PARTICLE RATIOS

As in the previous experiment [1] the fluxes of the most abundant particles ($\pi^{\pm}$, p, $\bar{p}$, $\Sigma^{\pm}$, Ξ^{-}) at the exit of the magnetic channel were directly measured with the DISC Čerenkov counter. Figures 1 and 2 show the DISC pressure curves for the negative and positive polarities, respectively. For the less abundant particles ($\bar{\Sigma}^{\pm}$, $\bar{\Xi}^{+}$, Ω^{-}, $\bar{\Omega}^{+}$), the fluxes could not be measured directly from the DISC pressure curves since the background counting rate of the Čerenkov counter was about 10^{-6} of the total beam flux. The rare hyperons were identified through their decay products, measured in the magnetic spectrometer triggered with the DISC set at the appropriate pressure [1,2]. To ensure identical geometrical acceptances for the decay products of the baryons and of the corresponding antibaryons, the polarity of the spectrometer magnet was reversed for the runs with positive beam polarity. The relevant decay channels were $\bar{\Sigma}^{+} \to \bar{p}\pi^{0}$ (34 events reconstructed with both gamma rays from the π^{0} detected), $\bar{\Xi}^{+} \to \bar{\Lambda}\pi^{+}$ (335 events), $\Omega^{-} \to \Lambda K^{-}$ (287 events), and $\bar{\Omega}^{+} \to$ $\to \bar{\Lambda}K^{+}$ (15 events). The methods used for selecting $\bar{\Xi}^{+}$ and $\bar{\Omega}^{+}$ events were identical to those used for Ξ^{-} and Ω^{-}, respectively [2]. For the last three decays, the

Λ ($\bar{\Lambda}$) was also reconstructed for all events in the samples. The reconstruction efficiency for $\overline{\Sigma^+} \to \bar{p}\pi^0$ was obtained by measuring the reconstruction efficiency for $\Sigma^+ \to p\pi^0$. For $\overline{\Xi^-}$, Ω^-, and $\overline{\Omega^-}$ decays, the reconstruction efficiency for the $\Xi^- \to \Lambda\pi^-$ events measured with the same total beam intensity was used. The relative acceptances of the spectrometer for the reconstructed decays have been calculated using a Monte Carlo simulation. The effective mass distributions for $\Xi^- \to \Lambda\pi^-$, $\overline{\Xi^-} \to \Lambda\pi^+$, $\Omega^- \to \Lambda K^-$, and $\overline{\Omega^-} \to \bar{\Lambda}K^+$ are shown in Figs. 3a-d. In a previous study [2] of the $\Omega^- \to \Lambda K^-$ decay, we have shown that there was a 2% background under the mass peak. We have taken this background level as an upper limit for the four decays listed above.

The particle-to-pion ratios at production have been calculated from the measured fluxes, taking into account the relative geometrical acceptances of the DISC, the decay lengths, the branching ratios, and reabsorption in the target. The corrections to the particle (antiparticle)-to-pion ratios arising from target reabsorption are only significant for the antibaryons since, compared to the baryons, their absorption cross-sections are larger and the production cross-sections fall very rapidly with increasing x. The reabsorption correction is largest for the ratio $\bar{p}/\pi^-$, being about 15% in this case. No corrections have been applied to the baryon-to-pion ratios. Since the corrections are small, our conclusions on production mechanisms are insensitive to their exact values. The measured baryon (antibaryon)-to-pion ratios are given in Table 1 and shown in Fig. 4. The straight lines are to guide the eye. Assuming the collisions to occur with free stationary nucleons, the kinematic variables corresponding to the data are:

$$\sqrt{s} = 21.2 \text{ GeV}, \quad p_T = 600 \text{ MeV/c}, \quad x = 0.48 ,$$

where $x = p_L^{cm}/p_{max}^{cm}$. Since we have not measured absolute cross-sections, the π^+/π^- ratio of 2.68 ± 0.05 was taken from the measurement of Singh et al. [3] at $\sqrt{s} = 45$ GeV, $x = 0.478$, and $0.45 \text{ GeV/c} \leq p_T \leq 0.65 \text{ GeV/c}$.

In the previous measurement at 100 GeV/c [1] the proportion of $\overline{\Sigma^-}$ in the Σ^+ triggers was determined by fitting the measured vertex distribution of the decays

Σ^+ ($\overline{\Sigma^-}$) $\rightarrow$ n ($\bar{n}$) + π^+, using the two known lifetimes. The ratio $\Sigma^+/\overline{\Sigma^-}$ at the DISC position, 12 metres from the production target, increases rapidly with momentum owing to the relative change in decay losses. Thus the procedure used to extract the $\overline{\Sigma^-}$ signal becomes less reliable at 113 GeV/c. For this reason the numbers given in Table 1 for $\overline{\Sigma^-}$ correspond to the 100 GeV/c measurement (p_T = 600 MeV/c, x = 0.48, but $\sqrt{s}$ = 19.8 GeV).

Statistical errors are significant only for $\overline{\Sigma}^{\pm}$, $\overline{\Xi^-}$, Ω^-, and $\overline{\Omega^-}$. Systematic errors arising from the variation of the production over the momentum acceptance are negligible. Care was taken to minimize possible effects on the DISC acceptance arising from changes in the settings of the proton beam and the magnetic channel. The systematic error from this source is estimated to be ±10% in all particle ratios. The exponential factors in the Ω^-/π^- and $\overline{\Omega^-}/\pi^-$ ratios come from the uncertainty in the Ω^- lifetime [τ_Ω = (0.822 ± 0.028) × 10^{-10} s (Ref. 2)]. This uncertainty does not affect the $\overline{\Omega^-}/\Omega^-$ ratio.

3. DISCUSSION

The results presented in Fig. 4 and in Table 1 show a rapid decrease of the B/π^- ratio with increasing baryon strangeness. The line drawn in the figure corresponds to $e^{-3.2|s|}$. To relate the variation of the inclusive production cross-section with strangeness observed in this experiment at x = 0.48 and p_T = = 0.6 GeV/c to the variation of the total inclusive cross-section, the x and p_T dependences must be taken into account.

In our earlier paper [1] it was shown that the x distributions for baryon production become steeper with increasing strangeness. However, compared to the cross-section integrated over all x, the fraction of the decrease observed at x = 0.48 due to this change of slope is less than a factor of 2 for each unit of strangeness.

The comparison of the results of this experiment with those of our previous measurement [1] made at the same value of x but at p_T = 0.2 GeV/c shows that the Σ^-/π^- ratio has increased by 18%, Ξ^-/π^- by 38%, and Ω^-/π^- by 44% between p_T = = 0.2 GeV/c and p_T = 0.6 GeV/c. These trends agree with the general observation

that the average value of p_T increases with the mass of the produced particle. Assuming the p_T distributions to be of the form $e^{-bp_T^2}$, the ratio between the production rate integrated over p_T and our measurement at p_T = 0.6 GeV/c is given by $I = \int[\exp(-bp_T^2)/\exp(-b\cdot 0.36)]dp_T^2$ which has a null derivative for b = = 2.8 $(GeV/c)^{-2}$. Over the range 2.3 $(GeV/c)^{-2} \leq b \leq 3.4$ $(GeV/c)^{-2}$ the integral I varies by only 2%. An observed typical value of b for Λ production at x = 0.5 is b = 2.8 $(GeV/c)^{-2}$ [4]. Even for b as low as 1 $(GeV/c)^{-2}$ the integral increases by only 40% with respect to the minimum value. Thus the effect of the increase of the average p_T as a function of the mass has a very small effect on the ratio $\sigma_{tot}(B)/[d\sigma(B)/dp_T^2]\big|_{p_T=0.6\,GeV/c}$ -- probably $\lesssim$ 10% between the proton and the Ω^-.

The decrease of the $\bar{B}/\pi^-$ ratio with increasing strangeness is not as strong as for baryons. The line drawn on the figure corresponds to $e^{-1.3|s|}$. The x distributions should be very similar for all antibaryons, and the effects arising from the variation of the average p_T with the mass of the particle are expected to be small, as in the baryon case.

The $\bar{B}/B$ ratio increases rapidly with strangeness. The line drawn in the figure corresponds to $e^{1.9|s|}$. Since the antibaryons have a much steeper x dependence than the baryons, the ratios between the antibaryon and the baryon integrated cross-sections are expected to be much larger than the values measured at x = 0.48. The ratio between the total inclusive cross-sections is estimated to be about 4.4% for $\bar{p}/p$ (see Section 4), and a rough estimate gives 75% for $\overline{\Omega^-}/\Omega^-$.

Baryons can be produced in the decay of excited states of the incoming proton (leading-particle effect) or by baryon-antibaryon pair production. The rapid increase of the antiparticle-to-particle production with strangeness can be interpreted in terms of the more rapid decline of the first process relative to the second one. In the next section we will make this discussion more rigorous by comparing our measurements with theoretical predictions, using additional experimental information where necessary.

4. INTERPRETATION OF THE DATA

Measurements of Λ and $\bar{\Lambda}$ production for various laboratory angles and momenta in proton-nucleus collisions at 300 GeV have been published by Skubic et al. [4]. The p_T dependences of the Λ and $\bar{\Lambda}$ production were found to be very similar. If the invariant cross-sections $E(d^3\sigma/dp^3)$ are represented by $(1 - x)^n$, then $n \simeq 7$ for $\bar{\Lambda}$ and $n \simeq 1$ (variable with x) for Λ. These data have been compared by Devlin et al. [5] with the predictions of a triple Regge model. Data taken in the same beam line by Edwards et al. [6], with 200 GeV π^-, K^-, $\bar{p}$, and p on beryllium, have been compared with the predictions of the constituent-interchange model of quark collisions. Both analyses show reasonable agreement with the theoretical predictions. However, these models cannot be easily applied to the production of Ξ^-, $\overline{\Xi^-}$, Ω^-, and $\overline{\Omega^-}$ in proton-nucleus collisions. In what follows we will attempt to interpret our measurements within the proton fragmentation-recombination model, using as a starting point the formulation of Kalinowski, Pokorski and Van Hove [7].

In this formulation there are six parameters A_1, A_2, A_3, η, η', and ξ, of which four are independent. Given an incident proton containing three valence quarks, A_1 is the probability that the three incident quarks emerge in three distinct outgoing hadrons; A_2 is the probability that the three incident quarks are shared between two outgoing hadrons; A_3 is the probability that the three quarks emerge in one outgoing baryon. The quantities η and η' are the probabilities that a *single* incident quark may recombine with non-incident antiquarks or quarks to form a meson with probability η, or a baryon with probability η'. With these definitions one has

$$A_1 + A_2 + A_3 = 1 \tag{1}$$

and

$$\eta + \eta' = 1 \ . \tag{2}$$

Finally, the probabilities for any non-incoming quark (or antiquark) to be strange, up, or down are ξ, $(1 - \xi)/2$, and $(1 - \xi)/2$, respectively (neglecting the production of heavier flavours). From our measurements [1] of the K^+/π^+ ratio at $x = 0.48$ and $x = 0.55$, we obtain with the equation $K^+/\pi^+ = 2\xi/(1 - \xi)$ a mean value of $\xi = 0.10 \pm 0.015$. Kalinowski et al. [7] have shown that η' is small.

Crucial tests of the model are provided by a comparison of the predictions with the experimental results for strange baryon and antibaryon production. We will discuss successively the antibaryon production, the proton and the s = -1 hyperon production, and the Ξ^- and Ω^- production.

4.1 The antibaryon production

The main diagram responsible for antibaryon production in the fragmentation region, according to the model, is shown in Fig. 5a. It is proportional to $A_2\ \eta'$. To first order in η' the mean multiplicities $\langle n_{\bar{B}} \rangle$ of the antibaryons produced in the fragmentation of the incoming proton ($x > 0$) are given by

$$\langle n_{\bar{p}} \rangle = \tfrac{1}{2}\ \eta' A_2 (1 - \xi)^3 \tag{3}$$

$$\langle n_{\bar{\Xi}^=} \rangle = \tfrac{3}{2}\ \eta' A_2 (1 - \xi)\xi^2 \tag{4}$$

$$\langle n_{\bar{\Omega}^=} \rangle = \eta' A_2 \xi^3 \ . \tag{5}$$

The mean multiplicity of s = +1 antibaryons is

$$\langle n_{s=+1} \rangle = 3\eta' A_2 (1 - \xi)^2 \xi \ ,$$

with $\langle n_{\bar{\Sigma}^=} \rangle + \langle n_{\bar{\Sigma}^+} \rangle = \langle n_{\bar{\Sigma}^0} \rangle + \langle n_{\bar{\Lambda}} \rangle$.

In the following we will use the mean multiplicity, $\langle n_{\bar{\Sigma}_{ch}} \rangle$, defined as:

$$\langle n_{\bar{\Sigma}_{ch}} \rangle = \langle n_{\bar{\Sigma}^=} \rangle + \langle n_{\bar{\Sigma}^+} \rangle = \tfrac{3}{2}\ \eta' A_2 (1 - \xi)^2 \xi \ . \tag{6}$$

Since all the fragmentation antibaryons are produced by the same diagram (Fig. 5a), the x and p_T dependences of their invariant cross-sections are expected to be the same. We can therefore make a direct comparison of our measurements [which were all made at the same average (x, p_T) values] with the predictions of the model. The observed and expected $\bar{B}/\pi^-$ ratios at $x = 0.48$ and $p_T = 600$ MeV/c are listed in Table 2. For the expected ratios, the measured $\bar{p}/\pi^-$ value is used as input, and the other $\bar{B}/\pi^-$ ratios are calculated from $\bar{p}/\pi^-$ using (3) to (6) and $\xi = 0.10$.

The table shows a clear disagreement between the observed and the expected $\bar{B}/\pi^-$ ratios, which increases with the antibaryon strangeness. Agreement would be reached by using a ξ value of 0.15 instead of 0.10. However, we shall see below

that such a large value of ξ would generate difficulties in the baryon sector. Assuming that, with $\xi = 0.10$, the model gives a good description of the fragmentation contribution to the antibaryon production, the observed disagreement suggests that there is an additional contribution from non-fragmentation antibaryon-baryon pairs, which could even be the dominant one. Such a possibility is mentioned by Kalinowski et al. [7], but they have assumed that this pair production would be concentrated in the central region $-0.1 \lesssim x \lesssim 0.1$. A detailed phenomenological study [8] has shown that all the antiproton distributions are well explained if one assumes that, owing to local quantum number conservation, an antiproton is always emitted accompanied very closely in momentum space by a nucleon. However, an unambiguous distinction between the pair and the fragmentation contributions to antibaryon production can only be achieved with correlation measurements. For example, in the case of $\overline{\Omega^-}$ production the fragmentation contribution would correspond to an $[\overline{\Omega^-}\Xi\Lambda(\Sigma)]$ system, whereas the pair production would give mainly $[\overline{\Omega^-}\Omega^-]$. The pair production is expected to depend mainly upon the mass of the system, rather than upon the strangeness of the antibaryon, which could explain the general trend shown by Table 2.

To compare the baryon data with the model, we need to integrate the measured cross-sections over x and p_T. In addition, to analyse the fragmentation contribution to baryon production we shall use the difference between the baryon and the antibaryon cross-sections to eliminate the pair contribution. Thus we also need to integrate the antibaryon cross-sections. In the Appendix we discuss the integration procedure which yields the average particle multiplicities $\langle n_i \rangle$ in the forward hemisphere, using our data and the measurements of Refs. [9]-[13] for p and $\bar{p}$ production and of Refs. [4], [6], and [14]-[17] for Λ and $\bar{\Lambda}$ production.

4.2 The production of protons and s = -1 hyperons

We now discuss the production of protons, Λ (Σ^0), Σ^+, and Σ^-. In the model of Kalinowski et al. [7] the particle multiplicities in the forward hemisphere are given by

$$\langle n_p \rangle = A_3 + \tfrac{2}{3} A_2(1 - \xi) + \tfrac{3}{2} (A_1 + \tfrac{1}{3} A_2)\eta'(1 - \xi)^2 + \tfrac{1}{2} A_1\eta^3(1 - \xi)^3 \quad (7)$$

$$\langle n_\Lambda \rangle = \xi\Big[\tfrac{2}{3} A_2 + 3 (A_1 + \tfrac{1}{3} A_2)\eta'(1 - \xi) + \tfrac{3}{2} A_1\eta^3(1 - \xi)^2\Big] \quad (8)$$

$$\langle n_{\Sigma^+} \rangle = \xi\Big[\tfrac{1}{3} A_2 + 2 (A_1 + \tfrac{1}{3} A_2)\eta'(1 - \xi) + \tfrac{3}{4} A_1\eta^3(1 - \xi)^2\Big] \quad (9)$$

$$\langle n_{\Sigma^-} \rangle = \xi\Big[(A_1 + \tfrac{1}{3} A_2)\eta'(1 - \xi) + \tfrac{3}{4} A_1\eta^3(1 - \xi)^2\Big] \ . \quad (10)$$

They correspond to the diagrams of Fig. 5a-d and, for the term A_3 of $\langle n_p \rangle$, to the non-fragmented proton. Using (1) and the values of the particle multiplicities (see Appendix and Table 3), we give a graphical representation of (7)-(10) in Fig. 6 for $\eta' = 0$, $\eta = 1$, and $\xi = 0.10$. To retain only the fragmentation contribution, we have subtracted from each particle multiplicity the corresponding antiparticle multiplicity. Note that, for $\eta' = 0$, (3)-(6) do not contribute to the antiparticle multiplicities which are in that case entirely due to the $\bar{B}$-B pair production. The bands shown in Fig. 6 correspond to the uncertainties on the multiplicities quoted in the Appendix. The Σ^+ and the $(\Lambda + \Sigma^0)$ bands overlap exactly. The intersection of the three bands gives $A_2 \simeq 0.6$ and $A_1 \simeq 0.15$. Using $A_2 = 0.6$ and the antiproton multiplicity given in Table 3, $\langle n_{\bar{p}} \rangle = 3.0 \times 10^{-2}$, we obtain from (3) a value of 0.13 for η'. This is certainly an upper limit, since a large fraction of the antiprotons should be due to pair production especially at small x where most of the multiplicity is concentrated. The values quoted above for A_2 and A_1 are still valid for $\eta' \lesssim 0.05$. The A_1 versus A_2 plot of Fig. 7 corresponds to $\eta = 1$ and $\eta' = 0$ as for Fig. 6, but with $\xi = 0.15$, a value suggested by the antiparticle ratios of Table 2. There is no overlap between the three bands drawn in Fig. 7 and therefore no acceptable solution.

4.3 The Ξ^- and Ω^- production

In the model of Kalinowski et al. [7] the Ξ^- and Ω^- multiplicities are

$$\langle n_{\Xi^-} \rangle = \xi^2\Big[\tfrac{3}{2} (1 - \xi)A_1\eta^3 + (A_1 + \tfrac{1}{3} A_2)\eta'\Big] \quad (11)$$

$$\langle n_{\Omega^-} \rangle = \xi^3 A_1\eta^3 \ . \quad (12)$$

Our data cover an x range which is too limited to allow an integration over x. The ratio Ω^-/Ξ^- at $x = 0.48$ and $p_T = 600$ MeV/c is $(1.9 \pm 0.5) \times 10^{-2}$. The

terms which contain $A_1\eta^3$ in $\langle n_{\Xi^-}\rangle$ and $\langle n_{\Omega^-}\rangle$ both correspond to the diagram of Fig. 5c and are therefore expected to have identical x and p_T dependences. The second term of (11) corresponds to the diagram of Fig. 5a, which also produces the antibaryons, and to the diagram of Fig. 5d. The measured ratio $\overline{\Xi^-}/\Xi^-$ at $x = 0.48$ and $p_T = 600$ MeV/c is $(3.75 \pm 0.45) \times 10^{-2}$. Using the values of A_1 and A_2 given in Section 4.2 to determine the coefficients of η' in $\langle n_{\Xi^-}\rangle$ and $\langle n_{\overline{\Xi^-}}\rangle$, we deduce from the measured $\overline{\Xi^-}/\Xi^-$ ratio that the η' term would contribute at most 1.5×10^{-2} of the observed Ξ^- at $p_T = 600$ MeV/c and $x = 0.48$ if the p_T and x dependences of the η' terms were the same for Ξ^- and $\overline{\Xi^-}$. With the $(1 - x)^7$ dependence of the antiparticle distributions and the observed $(1 - x)^3$ dependence for Ξ^- above $x = 0.48$, we may reasonably assume an enhancement factor of about $\frac{4}{8}\ (1-0.48)^{-4} = 6.8$ for the Ξ^- contribution. As already discussed in Section 3, we expect the contribution to the enhancement factor from the p_T dependence to be negligible. We therefore conclude that the contribution of the η' term amounts to about 10% of the observed Ξ^- at $p_T = 600$ MeV/c and $x = 0.48$. Neglecting this small contribution, (11) and (12) give:

$$\Omega^-/\Xi^- = \tfrac{2}{3}\ \xi/(1 - \xi)\ .$$

This is 7.4×10^{-2} for $\xi = 0.10$ and 12×10^{-2} for $\xi = 0.15$, in strong disagreement with the measured ratio of $(1.9 \pm 0.5) \times 10^{-2}$. Through all the above discussion we have assumed that all the Ξ^- and Ω^- produced at $x = 0.48$ were of the fragmentation type without a $B\bar{B}$ pair contribution, but, as shown in Section 3.1, such a contribution is a necessity for $\xi = 0.10$. The disagreement now becomes even worse since the pair contribution corresponds to a larger fraction of Ω^- than of Ξ^-. To account for the Ξ^- and Ω^- production the model must be modified.

Kalinowski et al. [7] have considered only a single fragmentation of the proton per collision. We shall now assume that successive fragmentations may occur within the same interaction. Examples of such multifragmentation (MF) contributions are shown in Fig. 8a,b*). We define a new coefficient A_2^{MF}, which is the sum of the probabilities for one or more successive fragmentations into two

*) We wish to emphasize that the diagrams of Fig. 8a, b are obtained by repeating the basic diagram of Fig. 5b within the same interaction. They are not reinterpretations of the diagrams of Fig. 5c, d, which still remain in the multifragmentation scheme.

hadrons. For simplicity we shall assume that the probabilities for each elementary fragmentation are the same and that they factorize. The A_2^{MF} probability can then be expressed as a function of the elementary probability a_2:

$$A_2^{MF} = a_2 + a_2^2 + \ldots = a_2/(1 - a_2) \ . \qquad (13)$$

From (13) one gets

$$a_2 = A_2^{MF}/(1 + A_2^{MF}) \ .$$

The main effect of the multifragmentation scheme for the s = -1 hyperon probabilities is to introduce a new A_2 term in $\langle n_{\Sigma^-} \rangle$. The effect of this term is shown in Fig. 6 where the two axes now correspond to the variables A_2^{MF} and A_1^{MF}. There are also small changes ($\sim$ 10%) for the A_2 contributions to the other mean multiplicities. Other higher-order terms such as $a_2 a_1$ can be neglected because of the small value of a_1.

The a_2 multifragmentation now becomes the dominant contribution to Ξ^- and Ω^- production at large x. The lowest-order diagrams are shown in Fig. 8a, and 8b for Ξ^- and Ω^-, respectively. Neglecting the other terms, the Ω^-/Ξ^- ratio at x = 0.48 is given by:

$$\Omega^-/\Xi^- = a_2 \xi \varepsilon \ ,$$

where the factor ε represents the effect of the different x dependences of the Ξ^- and Ω^- cross-sections. Since the observed dependence on x for Σ^- is $(1 - x)^{1.5}$ and for Ξ^- is $(1 - x)^3$, we assume a $(1 - x)^{4.5}$ dependence for Ω^- production. This is compatible with the measured invariant cross-sections [1] at x = 0.48 and x = 0.55. Using, in addition, the value $A_2^{MF} = 0.6$ we obtain $\Omega^-/\Xi^- = 1.8 \times 10^{-2}$ for $\xi = 0.10$ -- in agreement with the observed ratio -- and $\Omega^-/\Xi^- = 2.8 \times 10^{-2}$ for $\xi = 0.15$.

Including the multifragmentation contributions, we deduce a final set of parameters for $\xi = 0.10$:

$$A_1^{MF} \simeq 0.1 \ , \quad A_2^{MF} \simeq 0.6 \ , \quad A_3^{MF} \simeq 0.3$$

$$\eta' < 0.1 \quad \text{and} \quad \eta > 0.9 \ .$$

5. CONCLUSION

Data on the production of charged baryons and antibaryons in p-BeO collisions at $\sqrt{s}$ = 21 GeV, x = 0.48, and p_T = 600 MeV/c have been presented. They include measurements of the particle/negative-pion ratios of charged, $|s|$ = 0, 1, 2, 3, baryons and antibaryons. In particular this is the first measurement of the $\overline{\Omega^-}$ production rate.

The ratio antibaryon/baryon increases very quickly with strangeness, from 1.0×10^{-3} for $\bar{p}/p$ to about 3×10^{-1} for $\overline{\Omega^-}/\Omega^-$.

The results can be interpreted within the framework of the proton fragmentation-recombination model of Kalinowski et al. [7] with two important additions:

a) a large fraction (probably almost all) of the antibaryons arise from baryon-antibaryon pair production and not from a fragmentation process even at large x ($x \simeq 0.5$);

b) higher-order contributions corresponding to several successive fragmentations within the same interaction are essential to explain the Ξ^- and Ω^- production.

The three-quark system of the incident proton appears to fragment into two quarks and one quark about 60% of the time. It is fully broken into three separate quarks in only 10% of the cases, while in the remaining 30% the three quarks stay together. Such a model gives a comprehensive representation of our data on the production of charged baryons and antibaryons (s = -3 to +3).

APPENDIX

DETERMINATION OF THE AVERAGE PARTICLE MULTIPLICITIES IN THE FORWARD HEMISPHERE

The multiplicity $\langle n_i \rangle$ for each type of particle i is defined as:

$$\langle n_i \rangle = \frac{1}{\sigma_{inelastic}} \int \sigma_{inv}(i) \frac{dp^3}{E} \qquad (A.1)$$

where $\sigma_{inelastic}$ = 32 mb is the pp inelastic cross-section at $\sqrt{s}$ = 21 GeV, and $\sigma_{inv}(i) = E\, d^3\sigma/dp^3$ is the inclusive production cross-section. The integration extends over the forward hemisphere ($x \geq 0$). The invariant cross-section at $x = 0.48$ and p_T = 600 MeV/c is obtained from the measured ratios B/π^- (or $\bar{B}/\pi^-$) through the relation:

$$\sigma_{inv}(B) = (B/\pi^-) \times \sigma_{inv}(\pi^-) \ .$$

The value $\sigma_{inv}(\pi^-) = 0.264$ mb/GeV^2, measured by Singh et al. [3] at $\sqrt{s}$ = 45 GeV is used for our measurement at $\sqrt{s}$ = 21 GeV since $\sigma_{inv}(\pi^-)$ at large x does not vary within this $\sqrt{s}$ range [11].

The mean proton multiplicity is obtained from

i) the inclusive cross-section $p + p \rightarrow p + X$ measured in a hydrogen bubble chamber for $-1 < x < -0.6$ and an incident proton momentum of 205 GeV/c [9];

ii) the ISR measurements [10]-[12] of the invariant cross-section for $0 < x < 0.6$ which are integrated using the method of Antinucci et al. [18] and of Rossi et al. [19].

We find a value $\langle n_p \rangle = 0.74 \pm 0.06$ for the average proton multiplicity in the forward hemisphere in agreement with the calculation of Rossi et al. [19] which gives $\langle n_p \rangle = 0.81$ for $\sqrt{s}$ = 23.3 GeV (the values given in Ref. 19 are total multiplicities and must be divided by a factor of 2 for comparison). Since the integration is only required for part of the x range, the uncertainty on our determination of the proton multiplicity is reduced with respect to previous calculations which did not use the data from Ref. [9]. The protons produced in

Λ, $\bar{\Sigma}^+$, and Ξ^- decays are included in the ISR proton measurements. Subtracting these contributions (from our value $\langle n_p \rangle = 0.74$) and using the Λ and Σ^+ multiplicities calculated below, we obtain $\langle n_p \rangle = 0.68 \pm 0.06$.

The Λ production cross-section has been measured in several bubble chamber experiments using backward-produced Λ's [14]-[17]. Skubic et al. [4] have used their measurement to compute the integrated distribution $F(x) = (2/\pi\sqrt{s})$ $\int E_{cm}(d^2\sigma/dxdp_T^2)\, dp_T^2$. A comparison of these integrated distributions for the various experiments shows a deficiency of Λ's at low $|x|$ in all the bubble chamber experiments with respect to the counter experiments [4],[6]. This disagreement could arise from an insufficient correction for the loss of fast backward Λ's in the bubble chamber experiments. Using an average between the two types of measurements we get $\langle n_\Lambda \rangle = (6.3 \pm 0.9) \times 10^{-2}$, where the error has been enlarged to take into account the uncertainty mentioned above.

To determine the Σ^+ and Σ^- multiplicities, we have used the x dependence of the invariant cross-section given by Bourquin et al. [1] for $x \geq 0.5$ [$(1 - x)^{1.5}$ to be compared with $(1 - x)^{1.2}$ for Λ in the same x range (Refs. 4 and 6)]. For lower x values we have assumed the same x dependence as for Λ. The p_T dependence of the Λ cross-section has also been used. We obtain $\langle n_{\Sigma^+} \rangle = (3.0 \pm 0.5) \times 10^{-2}$ and $\langle n_{\Sigma^-} \rangle = (1.4 \pm 0.2) \times 10^{-2}$.

The Ω^- and Ξ^- data are too limited to allow a determination of their average multiplicities.

To evaluate the antiparticle multiplicities, we have used the following information and assumptions:

a) the p_T and x dependences of the invariant cross-sections have been measured by Capiluppi et al. [12] for antiprotons and by Skubic et al. [4] and Edwards et al. [6] for $\bar{\Lambda}$;

b) for all the other antihyperons we have assumed the same p_T and x dependences as measured for $\bar{\Lambda}$.

The integrand of (A.1) is written as $\sigma_{inv}(i)\pi\ (\sqrt{s}/2E_{cm})\ dxdp_T^2$, and the integration is performed in two steps:

i) the invariant cross-section is first integrated over p_T at x = 0.48;

ii) the result is then integrated over x replacing $\sqrt{s}/2E_{cm}$ using the approximation $\left[x^2 + 4(m_i^2 + \langle p_T^2 \rangle)/s\right]^{-1/2}$, where m_i is the particle mass and $\langle p_T^2 \rangle = \int \sigma_{inv}\, p_T^2\, dp_T^2 / \int \sigma_{inv}\, dp_T^2$.

Because of the large value of x at which our measurements have been obtained, the error introduced by the approximation is completely negligible.

All the computed multiplicities are given in Table 3. For $\overline{\Sigma^+}$ and $\overline{\Sigma^-}$ the value listed corresponds to $\langle n_{\overline{\Sigma}^+} \rangle + \langle n_{\overline{\Sigma}^-} \rangle$. Within the statistical accuracy of our data $\langle n_{\overline{\Sigma}^+} \rangle = \langle n_{\overline{\Sigma}^-} \rangle$.

The $\bar{p}$ multiplicity $\langle n_{\bar{p}} \rangle = 4.3 \times 10^{-2}$ calculated by Rossi et al. [19] at $\sqrt{s} = 23.3$ GeV includes the contribution from $\bar{\Lambda}$, $\overline{\Sigma^+}$, $\overline{\Xi^-}$, and $\overline{\Omega^-}$ decays. Using our results at $\sqrt{s} = 21.2$ GeV, we get 4.2×10^{-2} for the $\bar{p}$ multiplicity, if we also include the $\bar{p}$ contributions from these decay sources.

We estimate the accuracy on the antibaryon multiplicities to be 20% for $\bar{\Lambda}$, $\bar{p}$, and $\overline{\Xi^-}$, 30% for $\bar{\Sigma}$, and about 35% for $\overline{\Omega^-}$.

REFERENCES

[1] M. Bourquin, R.M. Brown, Y. Chatelus, J.C. Chollet, M. Croissiaux, A. Degré, M. Ferro-Luzzi, D. Froidevaux, A.R. Fyfe, J.-M. Gaillard, C.N.P. Gee, W.M. Gibson, R.J. Gray, P. Igo-Kemenes, P.W. Jeffreys, B. Merkel, R. Morand, R.J. Ott, H. Plothow, J.-P. Repellin, B.J. Saunders, G. Sauvage, B. Schiby, H.W. Siebert, V.J. Smith, K.-P. Streit, R. Strub, J.J. Thresher and J. Trischuk, Nucl. Phys. B153, 13 (1979).

[2] M. Bourquin, R.M. Brown, Y. Chatelus, J.C. Chollet, A. Degré, D. Froidevaux, A.R. Fyfe, C.N.P. Gee, J.-M. Gaillard, W.M. Gibson, P. Igo-Kemenes, P.W. Jeffreys, B. Merkel, R. Morand, H. Plothow, J.-P. Repellin, B.J. Saunders, G. Sauvage, B. Schiby, H.W. Siebert, V.J. Smith, K.-P. Streit, R. Strub, J.J. Thresher and S.N. Tovey, Phys. Lett. 87B, 297 (1979).

[3] J. Singh, M.G. Albrow, D.P. Barber, P. Benz, B. Bošnjaković, C.Y. Chang, A.B. Clegg, F.C. Erné, P. Kooijman, F.K. Loebinger, N.A. McCubbin, P.G. Murphy, A. Rudge, J.C. Sens, A.L. Sessoms and J. Timmer, Nucl. Phys. B140, 189 (1978).

[4] P. Skubic, O.E. Overseth, K. Heller, M. Sheaff, L. Pondrom, P. Martin, R. March, R. Handler, G. Bunce, P. Yamin, L. Schachinger, J. Norem, R.T. Edwards, B. Edelman and T. Devlin, Phys. Rev. D 18, 3115 (1978).

[5] T. Devlin, B. Edelman, R.T. Edwards, J. Norem, L. Schachinger, P. Yamin, G. Bunce, R. Handler, R. March, P. Martin, L. Pondrom, M. Sheaff, K. Heller, O.E. Overseth and P. Skubic, Nucl. Phys. B123, 1 (1977).

[6] R.T. Edwards, T. Devlin, B. Edelman, L. Schachinger, G. Bunce, R. Handler, P. Martin, L. Pondrom, M. Sheaff, P.T. Cox, K. Heller, O.E. Overseth, P. Skubic, R. Grobel, U. Nauenberg and K. Wild, Phys. Rev. D 18, 76 (1978).

[7] J. Kalinowski, S. Pokorski and L. Van Hove, Z. Phys. C, Particles and Fields 2, 85 (1979).

[8] M. Bourquin and J.-M. Gaillard, Nucl. Phys. B114, 334 (1976).

[9] S.J. Barish, D.C. Colley, P.F. Schultz and J. Whitmore, Phys. Rev. Lett. 31, 1080 (1973), and Phys. Rev. D 11, 3124 (1975).

[10] M.G. Albrow, A. Bagchus, D.P. Barber, A. Bogaerts, B. Bošnjaković, J.R. Brooks, A.B. Clegg, F.C. Erné, C.N.P. Gee, D.H. Locke, F.K. Loebinger, P.G. Murphy, A. Rudge and J.C. Sens, Nucl. Phys. B73, 40 (1974).

[11] B. Alper, H. Böggild, P. Booth, F. Bulos, L.J. Carroll, G. Damgaard, G. Von Dardel, B. Duff, K.H. Hansen, F. Heymann, J.N. Jackson, G. Jarlskog, L. Jönsson, A. Klovning, L. Leistam, E. Lillethun, E. Lohse, G. Lynch, G. Manning, K. Potter, M. Prentice, P. Sharp, S. Sharrock, S. Ølgaard-Nielsen, D. Quarrie and J.M. Weiss, Nucl. Phys. B100, 237 (1975).

[12] P. Capiluppi, G. Giacomelli, A.M. Rossi, G. Vannini and A. Bussière, Nucl. Phys. B70, 1 (1974).

[13] M.G. Albrow, A. Bagchus, D.P. Barber, A. Bogaerts, B. Bošnjaković, J.R. Brooks, A.B. Clegg, F.C. Erné, C.N.P. Gee, D.H. Locke, F.K. Loebinger, P.G. Murphy, A. Rudge, J.C. Sens and F. van der Veen, Nucl. Phys. B56, 333 (1973).

[14] G. Charlton, Y. Cho, D. Colley, M. Derrick, R. Engelmann, T. Fields, L. Hyman, K. Jaeger, U. Mehtani, B. Musgrave, Y. Oren, D. Rhines, P. Schreiner, H. Yuta, L. Voyvodic, R. Walker, J. Whitmore, H.B. Crawley, Z. Ming Ma and R.G. Glasser, Phys. Rev. Lett. 30, 574 (1973).

[15] F.T. Dao, D. Gordon, J. Lach, E. Malamud, J. Schivell, T. Meyer, R. Poster, P.E. Schlein and W.E. Slater, Phys. Rev. Lett. 30, 1151(1973).

[16] A. Sheng, V. Davidson, A. Firestone, F. Nagy, C. Peck, F.T. Dao, R. Hanft, J. Lach, E. Malamud, F. Nezrick, A. Dzierba and R. Poster, Phys. Rev. D 11, 1733 (1975).

[17] K. Jaeger, D. Colley, L. Hyman and J. Rest, Phys. Rev. D 11, 2405 (1975).

[18] M. Antinucci, A. Bertin, P. Capiluppi, M. D'Agostino-Bruno, A.M. Rossi, G. Vannini, G. Giacomelli and A. Bussière, Nuovo Cimento Lett. 6, 121 (1973).

[19] A.M. Rossi, G. Vannini, E. Albini, D. D'Alessandro and G. Giacomelli, Nucl. Phys. B84, 269 (1975).

Table 1

Particle ratios at $\sqrt{s}$ = 21.2 GeV, x = 0.48, and p_T = 600 MeV/c

B	B/π^-	$\bar{B}/\pi^-$	$\bar{B}/B$
p	12.1 ± 1.2	$(1.21 \pm 0.12) \times 10^{-2}$	$(1.0 \pm 0.1) \times 10^{-3}$
Σ^-	$(2.72 \pm 0.27) \times 10^{-1}$	$(3.5 \pm 0.9) \times 10^{-3}$	$(1.3 \pm 0.3) \times 10^{-2}$
Σ^+	$(7.30 \pm 0.73) \times 10^{-1}$	$(2.6 \pm 0.5) \times 10^{-3}$	$(3.6 \pm 0.6) \times 10^{-3}$
Ξ^-	$(2.93 \pm 0.29) \times 10^{-2}$	$(1.10 \pm 0.12) \times 10^{-3}$	$(3.75 \pm 0.45) \times 10^{-2}$
Ω^-	$(5.6 \pm 0.7) \times 10^{-4} \times e^{\pm 0.23}$	$(1.6 \pm 0.4) \times 10^{-4} \times e^{\pm 0.23}$	$(2.8 \pm 0.8) \times 10^{-1}$
$\frac{\Sigma^- + \Sigma^+}{2}$	$(5.01 \pm 0.50) \times 10^{-1}$	$(3.1 \pm 0.5) \times 10^{-3}$	$(6.2 \pm 1.3) \times 10^{-3}$

Table 2

Observed and expected $\bar{B}/\pi^-$ ratios at $\sqrt{s}$ = 21.2 GeV, x = 0.48, and p_T = 600 MeV/c

$\bar{B}/\pi^-$	$\bar{p}/\pi^-$	$\overline{\Sigma_{ch}}/\pi^-$	$\overline{\Xi^-}/\pi^-$	$\overline{\Omega^-}/\pi^-$
Observed	$(1.21 \pm 0.12) \times 10^{-2}$	$(6.2 \pm 1.0) \times 10^{-3}$	$(1.10 \pm 0.12) \times 10^{-3}$	$(1.6 \pm 0.5) \times 10^{-4}$
Expected	$(1.21 \pm 0.12) \times 10^{-2}$ input	$(4.1 \pm 0.4) \times 10^{-3}$	$(0.47 \pm 0.05) \times 10^{-3}$	$(0.36 \pm 0.04) \times 10^{-4}$
$\frac{\text{Observed}}{\text{Expected}}$	1	1.50 ± 0.28	2.33 ± 0.34	4.5 ± 1.5

Table 3

Average particle multiplicities in the forward hemisphere at $\sqrt{s}$ = 21.2 GeV

	p	Λ	Σ^+	Σ^-	Ξ^-	Ω^-
$\langle n_B \rangle$	0.68	6.3×10^{-2}	3.0×10^{-2}	1.4×10^{-2}	-	-
$\langle n_{\bar{B}} \rangle$	3.0×10^{-2}	1.3×10^{-2}	$\langle n_{\bar{\Sigma}^+} \rangle + \langle n_{\bar{\Sigma}^-} \rangle = 1.0 \times 10^{-2}$		1.9×10^{-3}	3.0×10^{-4}

Figure captions

Fig. 1 : DISC pressure curve with circular diaphragm [1] for 113 GeV/c negatively charged particles.

Fig. 2 : DISC pressure curve with circular diaphragm [1] for 113 GeV/c positively charged particles.

Fig. 3 : Effective mass distributions for: a) $\Xi^- \to \Lambda\pi^-$, b) $\overline{\Xi^-} \to \bar{\Lambda}\pi^+$, c) $\Omega^- \to \Lambda K^-$, d) $\overline{\Omega^-} \to \bar{\Lambda}K^+$.

Fig. 4 : Baryon/π^-, antibaryon/π^-, and antibaryon/baryon ratios as a function of the baryon (antibaryon) strangeness at $x = 0.48$ and $p_T = 600$ MeV/c. The straight lines have been drawn to guide the eye.

Fig. 5 : Fragmentation diagrams for the production of antibaryons and baryons. The diagrams drawn correspond to the lowest order (0 or 1) in η', the baryon recombination probability.

Fig. 6 : Graphical representation of the proton and s = -1 hyperon average multiplicities in the A_2A_1 plane for $\xi = 0.10$. The line labelled Σ^- (MF) is explained in Section 3.3.

Fig. 7 : Graphical representation of the proton and s = -1 hyperon average multiplicities in the A_2A_1 plane for $\xi = 0.15$.

Fig. 8 : Higher-order fragmentation diagrams corresponding to Ξ^- and Ω^- production.

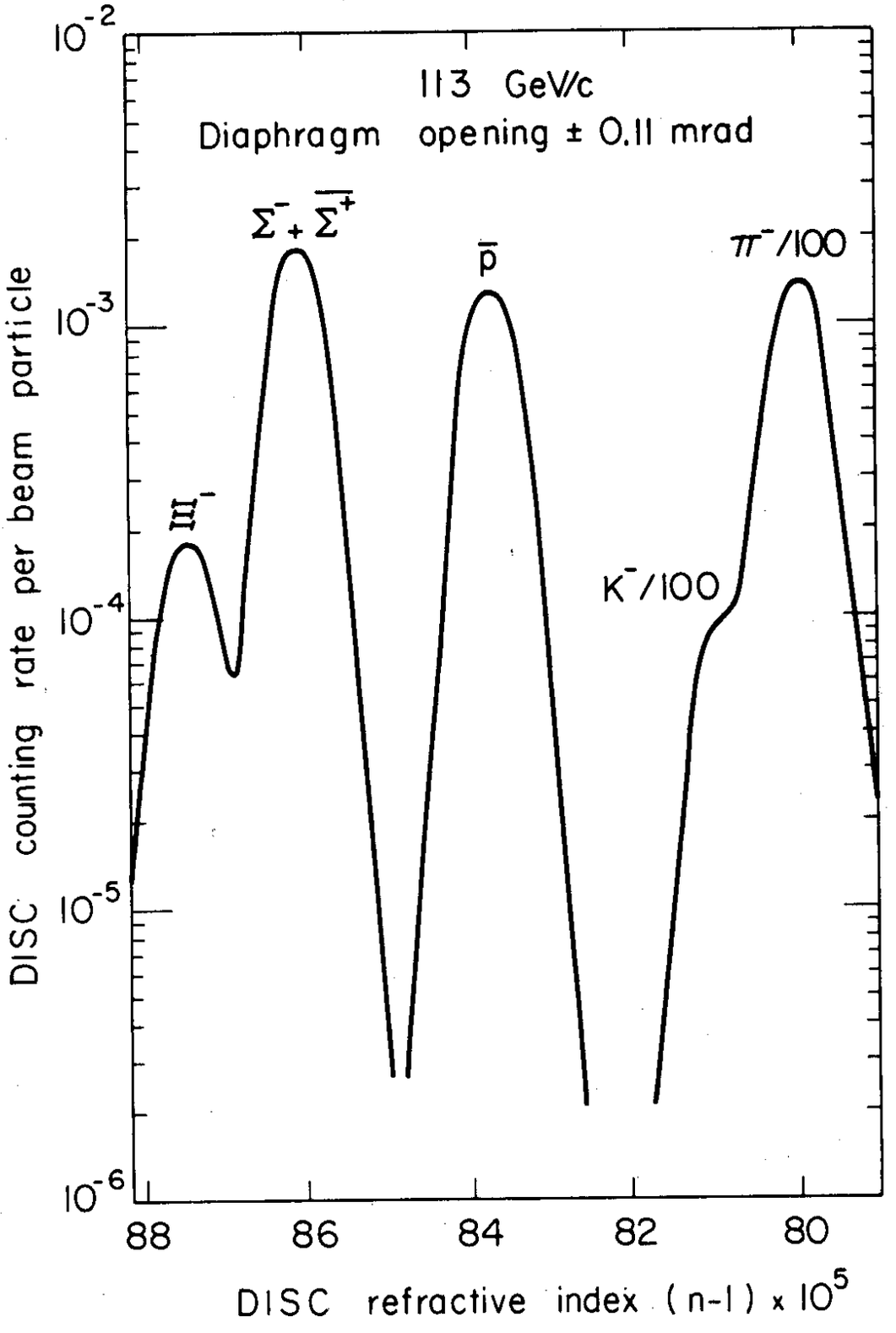
113 GeV/c
Diaphragm opening ± 0.11 mrad
$\Sigma^- + \overline{\Sigma^+}$
$\bar{p}$
$\pi^-/100$
Ξ^-
$K^-/100$
10^{-2}
10^{-3}
10^{-4}
10^{-5}
10^{-6}
DISC counting rate per beam particle
88
86
84
82
80
DISC refractive index (n-1) x 10^5

Fig. 1

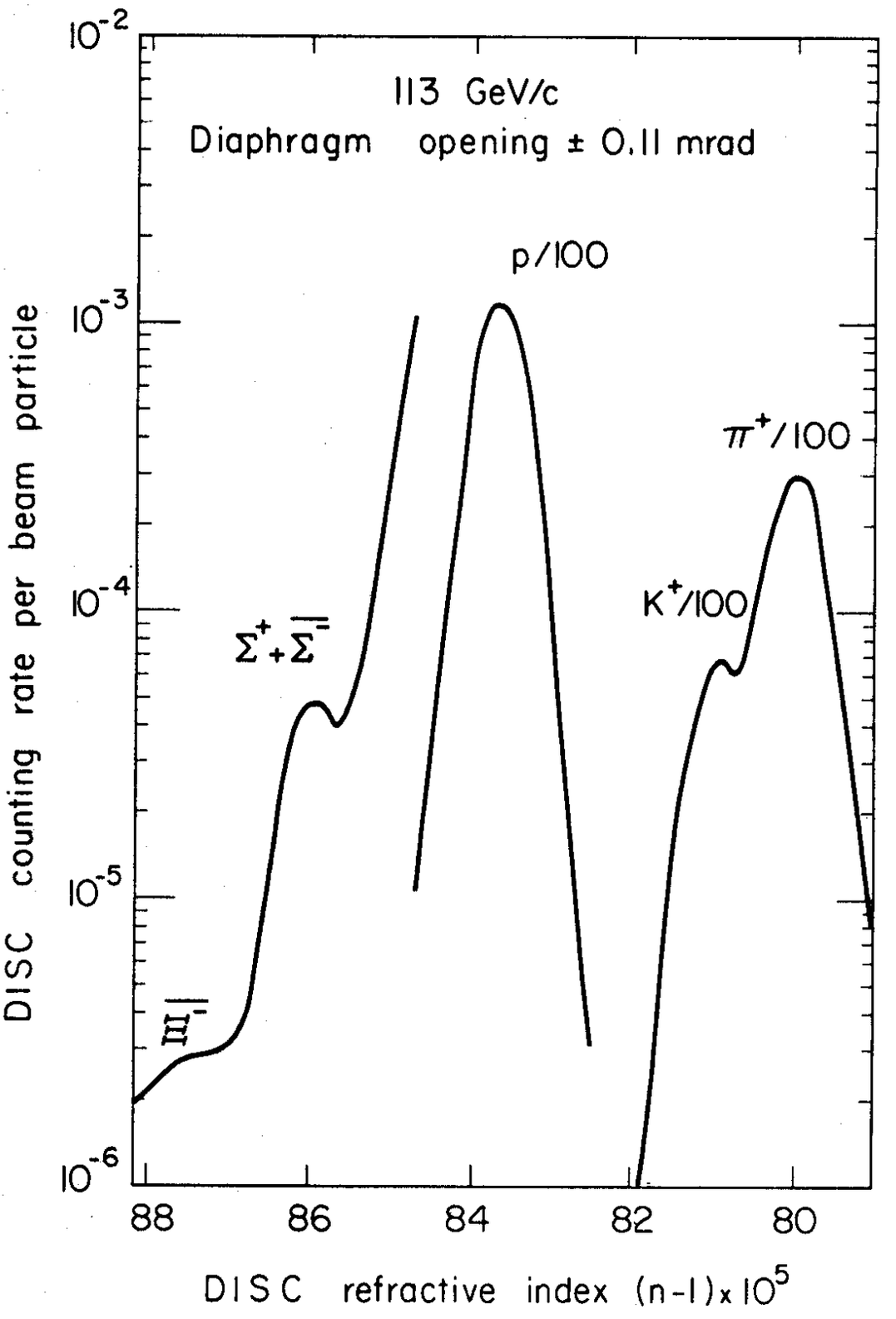
113 GeV/c
Diaphragm opening ± 0.11 mrad
p/100
π^+/100
K^+/100
$\Sigma^+ + \bar{\Sigma}^-$
Ξ^-
10^{-2}
10^{-3}
10^{-4}
10^{-5}
10^{-6}
DISC counting rate per beam particle
88
86
84
82
80
DISC refractive index $(n-1)\times 10^5$

Fig. 2

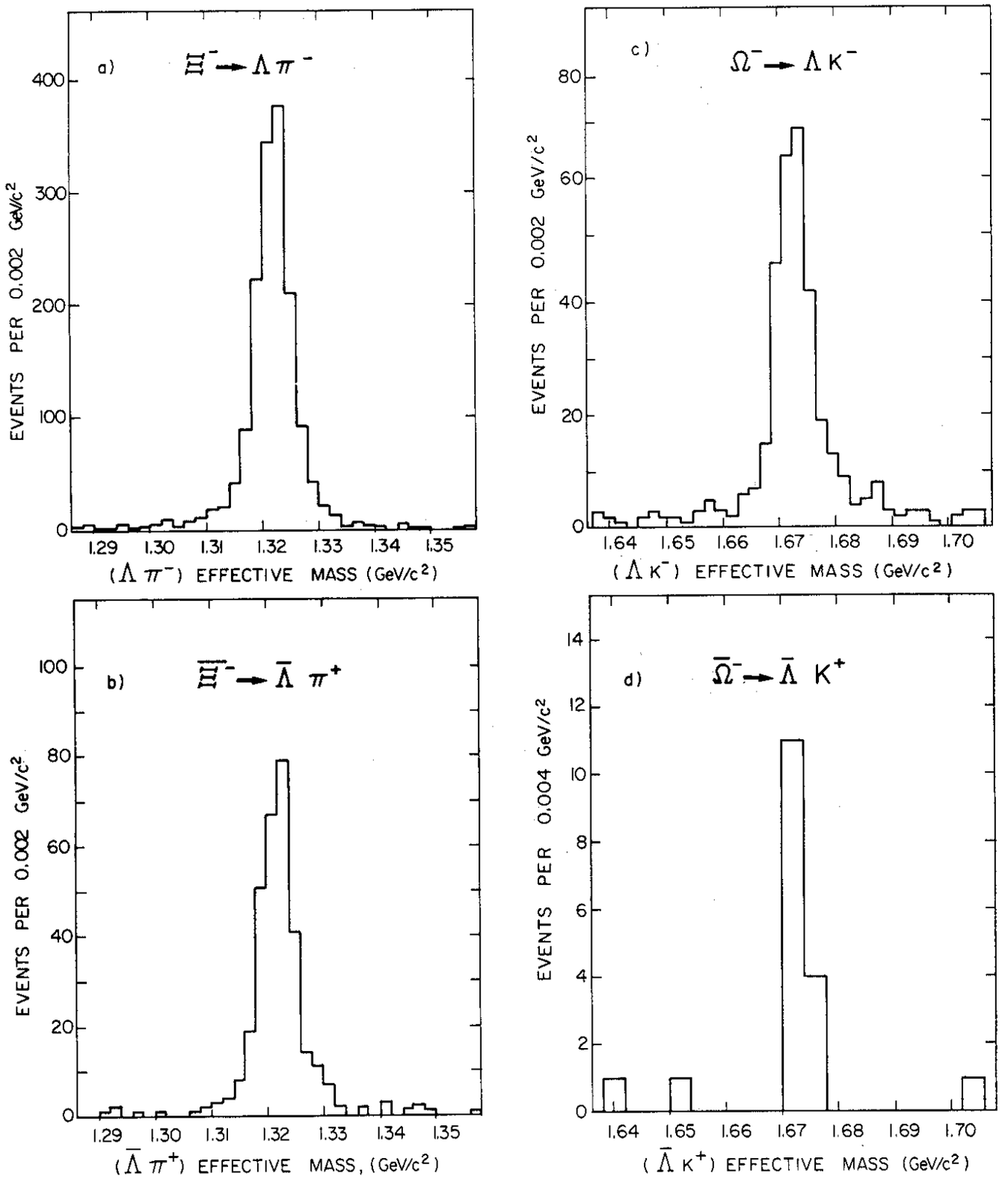
a) $\Xi^- \rightarrow \Lambda \pi^-$
EVENTS PER 0.002 GeV/c²
($\Lambda \pi^-$) EFFECTIVE MASS (GeV/c²)
b) $\bar{\Xi}^+ \rightarrow \bar{\Lambda} \pi^+$
EVENTS PER 0.002 GeV/c²
($\bar{\Lambda} \pi^+$) EFFECTIVE MASS, (GeV/c²)
c) $\Omega^- \rightarrow \Lambda K^-$
EVENTS PER 0.002 GeV/c²
(ΛK^-) EFFECTIVE MASS (GeV/c²)
d) $\bar{\Omega}^+ \rightarrow \bar{\Lambda} K^+$
EVENTS PER 0.004 GeV/c²
($\bar{\Lambda} K^+$) EFFECTIVE MASS (GeV/c²)

Fig. 3

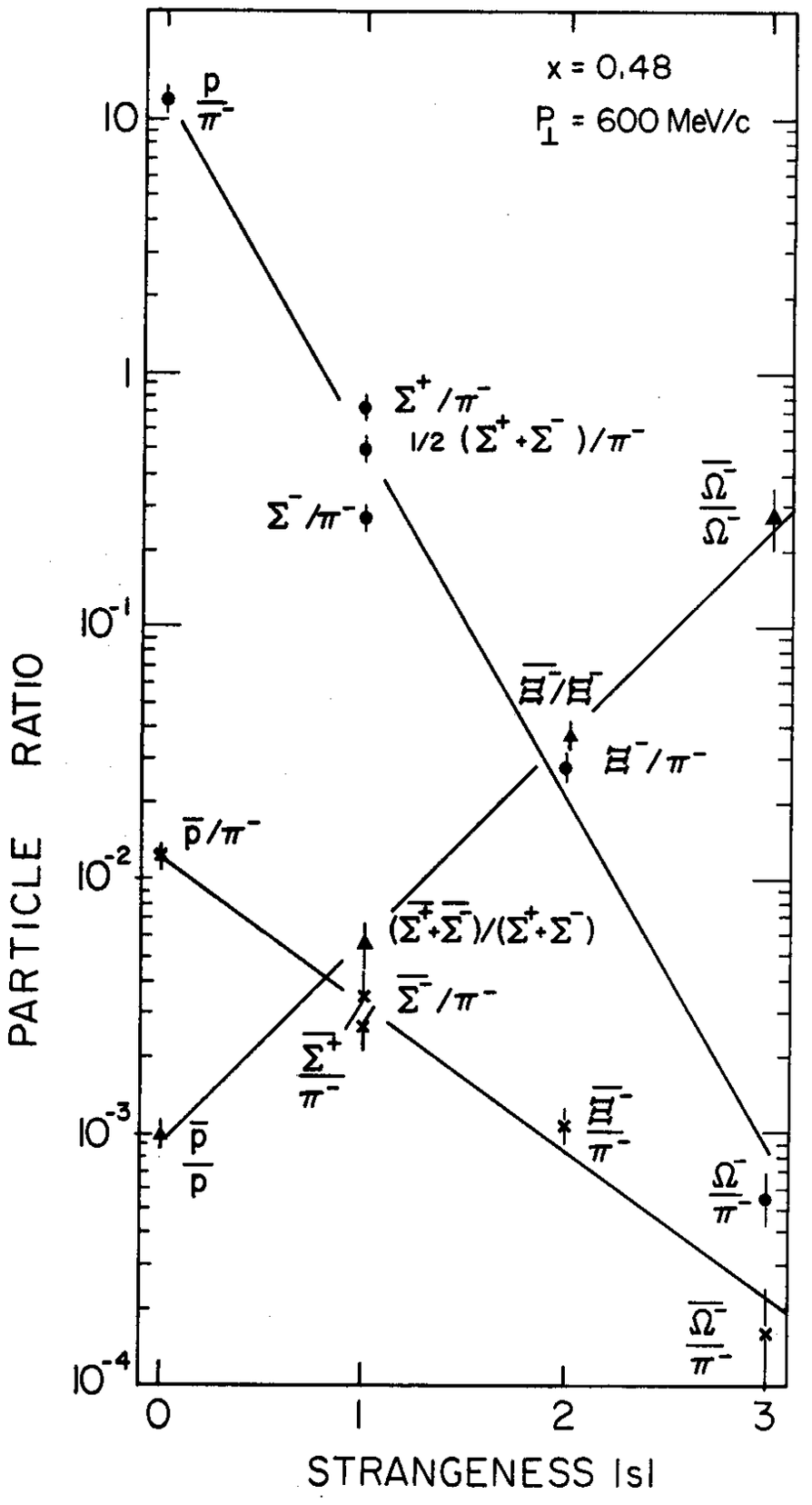
x = 0.48
P⊥ = 600 MeV/c
PARTICLE RATIO
STRANGENESS |s|
10
1
10⁻¹
10⁻²
10⁻³
10⁻⁴
0
1
2
3
p/π⁻
Σ⁺/π⁻
1/2 (Σ⁺+Σ⁻)/π⁻
Σ⁻/π⁻
Ω⁻/Ω⁻
Ξ⁻/Ξ⁻
Ξ⁻/π⁻
p̄/π⁻
(Σ⁺+Σ⁻)/(Σ⁺+Σ⁻)
Σ⁻/π⁻
Σ⁺/π⁻
p̄/p
Ξ⁻/π⁻
Ω⁻/π⁻
Ω⁻/π⁻

Fig. 4

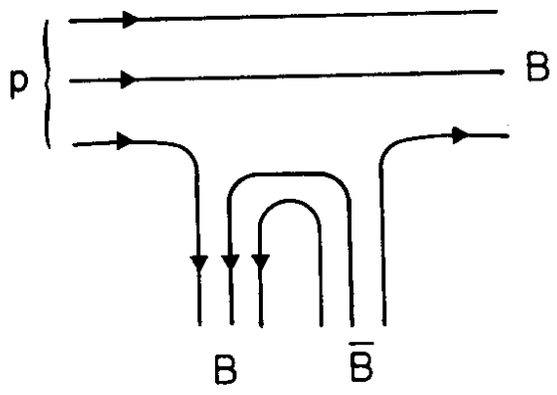

(a)

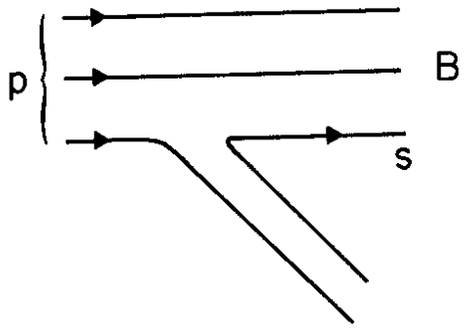

(b)

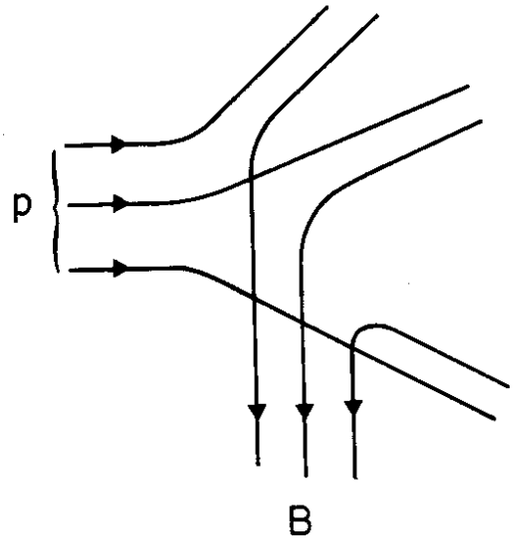

(c)

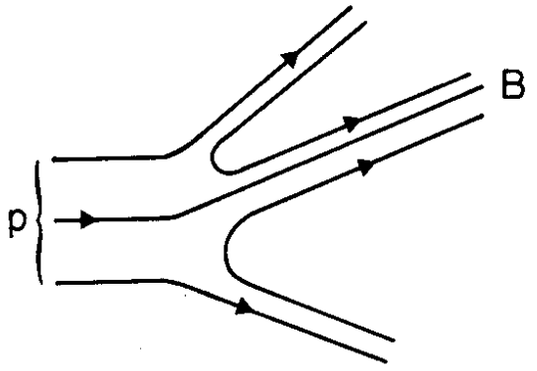

(d)

Fig. 5

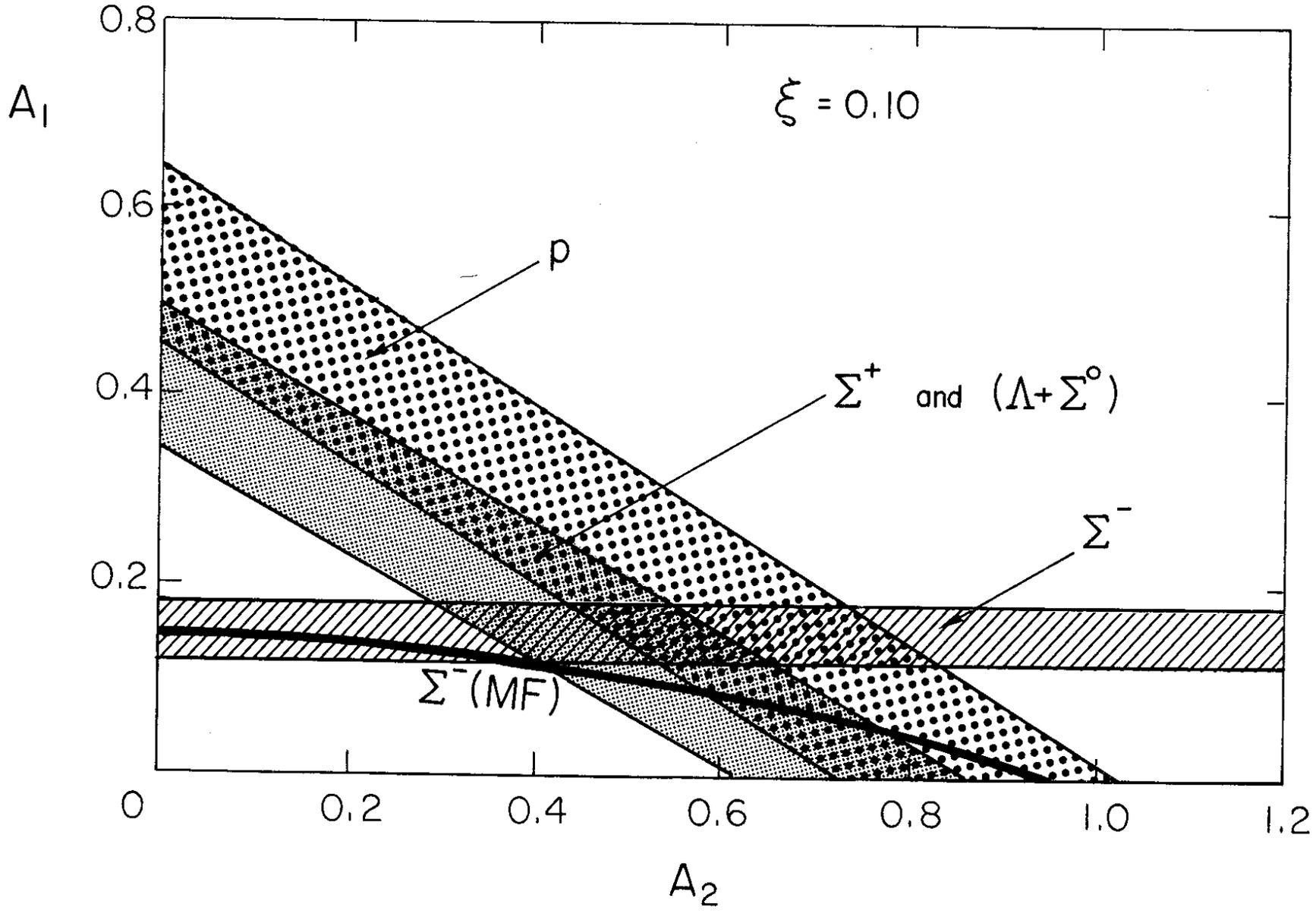
0.8
0.6
0.4
0.2
0
A_1
$\xi = 0.10$
p
Σ^+ and $(\Lambda+\Sigma^\circ)$
Σ^-
Σ^-(MF)
0.2
0.4
0.6
0.8
1.0
1.2
A_2

Fig. 6

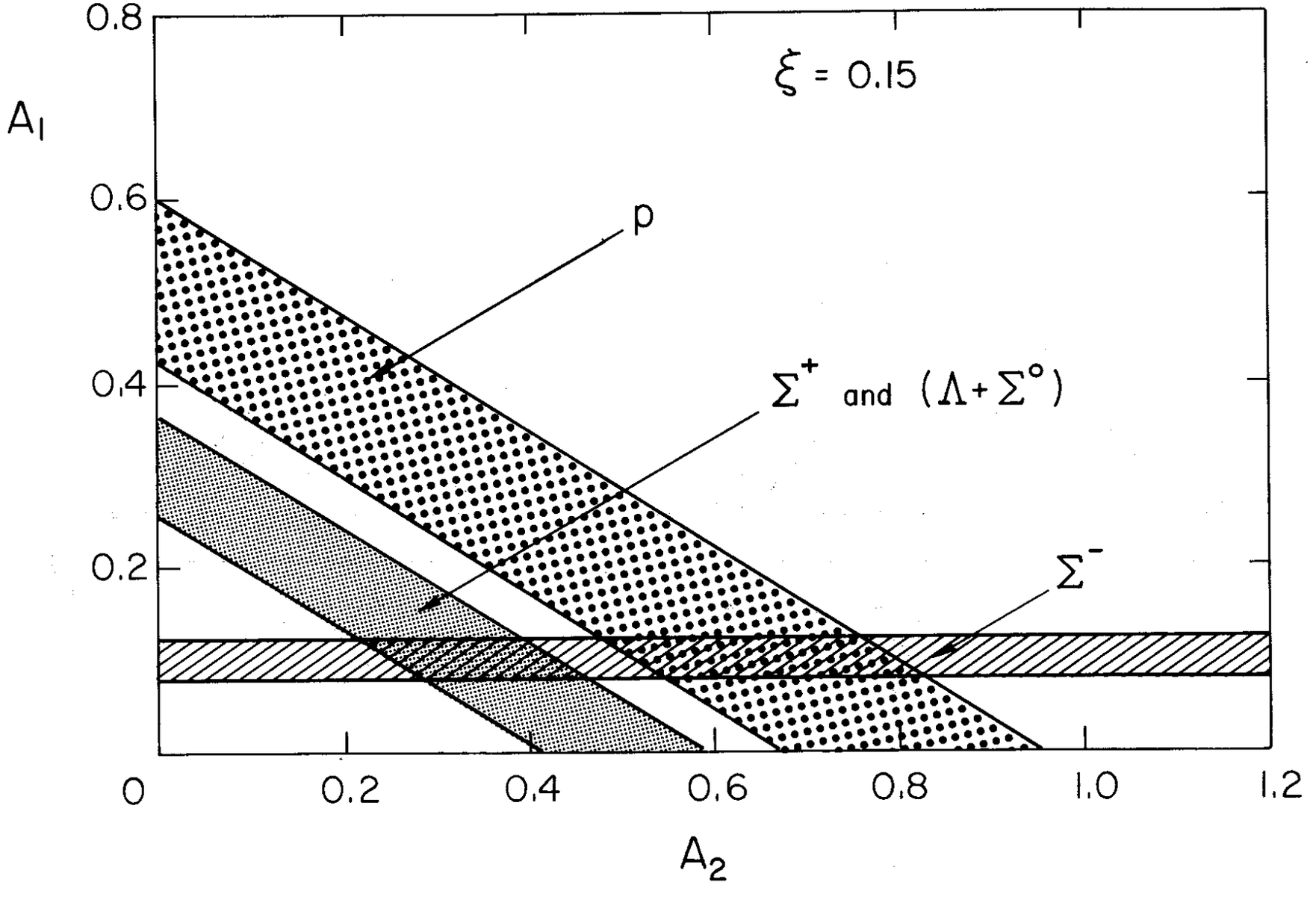
0.8
0.6
0.4
0.2
0
0.2
0.4
0.6
0.8
1.0
1.2
A_1
A_2
$\xi = 0.15$
p
Σ^+ and $(\Lambda + \Sigma^\circ)$
Σ^-

Fig. 7

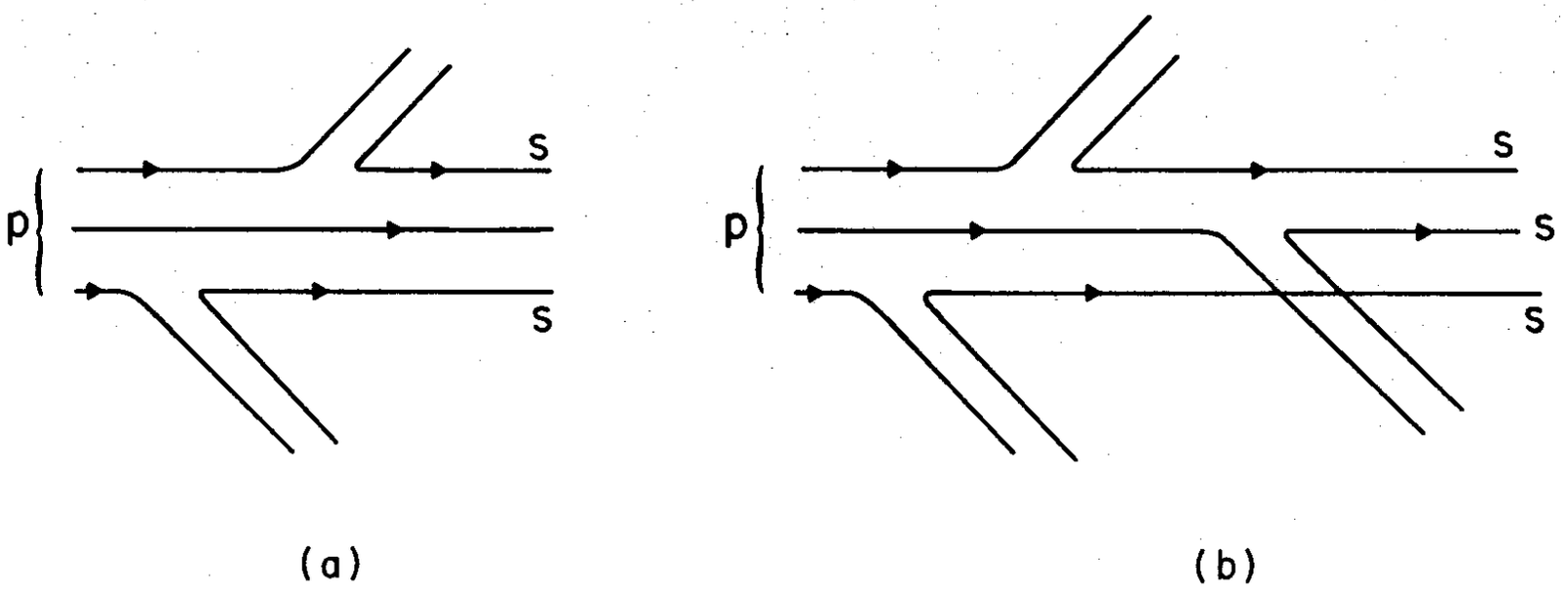

(a) (b)

Fig. 8